Applied Mathematics and Mechanics
(English Edition, Vol 25, No 1, Jan 2004)

Published by Shanghai University, Shanghai, China

 Article ID: 0253-4827(2004)01-0093-09

FOREBODY COMPRESSIBILITY RESEARCH OF HYPERSONIC VEHICLE*

LIU Jia (刘 嘉), YAO Wen-xiu (姚文秀)

LEI Mai-fang (雷麦芳), WANG Fa-min (王发民)

(Institute of Mechanics, Chinese Academy of Sciences, Beijing 100080, P. R. China)

(Communicated by BIAN Yin-gui, Original Member of Editorial Committee, AMM)

Abstract: Three kinds of forebody model of hypersonic vehicles were studied with numerical simulation method. It shows that the two-order compressive ramp model is the best selection among the three for its good evaluative parameters value at the cowl of the inlet. This model can provide higher value of flux coefficient and total pressure recovery coefficient and lower average Mach number compared with those of the other two models. Simultaneously different compressive angles may have different effects. The configuration which the first-order of compressive angle is 4° and the second 5° is the optimum combination. Furthermore factors such as attack angle were concerned. Better result may be obtained with a range of attack angles. Based on the work above the integrated design for forebody/inlet of a hypersonic vehicle was performed. The numerical result shows that this integrated model provides good flow field quality for inlet and engine work.

Key words: hypersonic vehicle; integration of forebody-inlet; compressibility

Chinese Library Classification: V211 Document code: A

2000 Mathematics Subject Classification: 76K05

Introduction

The integrated design of airframe/propulsion of hypersonic vehicle is one of the key technology for the air-breathing engine hypersonic vehicles[1~4]. The purposes to do integrated design of forebody/inlet are to put the forebody as the pre-compressive ramp, to provide uniform flow field, which means small pressure and velocity gradient, small oriental angle of gas flow and low average Mach number at the entry of the inlet, and enough flux for the inlet, furthermore to meet the design request of inlet. On the other hand, it must be non-sensitive to the Mach number and attack angle in order to avoid aberrance on offdesign condition[5].

O'Neill and Lewis[6,7] investigated the method of integrated design based on waverider configuration generated with a conical shock. He indicated that the performance of the hypersonic

* Received date: 2002-05-30; Revised date: 2003-07-31

Biographies: LIU Jia (1970~), Doctor (E-mail: liujia2003@hotmail.com);

WANG Fa-min (Corresponding author) (Tel: 86-010-62537660; Fax: 86-010-62651284; E-mail: wangfm@imch.ac.cn)

cruise vehicle and accelerated vehicle is affected by the uniformity of the flow field greatly. Uniformity of mass flow, pressure and temperature distribution is important for the efficient combustion. It is the forebody of the vehicle who provides the flow field for the inlet, so the flow field should be pr-compressed and be uniform for spanwise and vertical direction.

The Mach 10 cruise vehicle configuration of lifting body was studied in NASA Langley Research Center[8]. The result shows that the combination of forebody and four compressive ramps is optimum. This configuration may be composed of flat cowl and the reflection shock reaches the shoulder of the inlet. Putting the cowl lowerly and reset the four ramps we can get better flow capture. Simultaneously through the research of the turnup cowl, they found that it weakens the cowl shock at some extent and enhances the drag force.

In this paper, the characteristic of flow field of three different models is investigated by numerical simulation method. The evaluative parameters are calculated at the entry of the inlet. It shows that the two-order compressive model is optimum for the hypersonic vehicle. Furthermore we study the affection of thes attack angle and effect of different combinations of compressive angles. It proves that the two order-compressive model is a useful and efficient model for hypersonic vehicle forebody design at rational combination of compressive angles and a range of attack angle.

1 Control Equations and Numerical Method

Nondimensional integral N-S (Navier-Stokes) equation is as follows:

$$\begin{cases} \iiint_{\Omega} \frac{\partial}{\partial t}\rho \mathrm{d}\Omega + \oint_{\Gamma}\rho \mathbf{q}\cdot\mathrm{d}\mathbf{S} = 0, \quad \iiint_{\Omega} \frac{\partial}{\partial t}\rho \mathbf{q}\mathrm{d}\Omega + \oint_{\Gamma}\rho \mathbf{q}(\mathbf{q}\cdot\mathrm{d}\mathbf{S}) = \oint_{\Gamma}\boldsymbol{\tau}_n\cdot\mathrm{d}\mathbf{S}, \\ \iiint_{\Omega} \frac{\partial}{\partial t}e\mathrm{d}\Omega + \oint_{\Gamma}e(\mathbf{q}\cdot\mathrm{d}\mathbf{S}) = \oint_{\Gamma}\boldsymbol{\tau}_n\cdot\mathrm{d}\mathbf{S} + \oint_{\Gamma}C\frac{\partial}{\partial n}(p/\rho)\mathrm{d}S, \\ p = (\gamma - 1)\left(e - \frac{1}{2}\rho q^2\right), \quad \boldsymbol{\tau} = -\left(p + \frac{2}{3}\mu\mathrm{div}(\mathbf{q})\right)\mathrm{I} + \mu\boldsymbol{\varepsilon}. \end{cases} \tag{1}$$

Here Γ is the boundary surface of the control volume Ω, $C = \gamma/(\gamma - 1)\cdot\mu/p_r$, $p_r = \mu c_p/k\lambda$, $\boldsymbol{\tau}_n$ is the stress on the unit area of a tiny area $\mathrm{d}S$ and $\boldsymbol{\varepsilon}$ is the strain tensor.

Equation (1) becomes a discrete equation on a tiny volume,

$$V_{i,j,k}\cdot\frac{\mathrm{d}U_{i,j,k}}{\mathrm{d}t} = -R_{i,j,k} + R_{Vi,j,k}, \tag{2}$$

where $U_{i,j,k} = 1/V_{i,j,k}\iiint_{\Omega} U\mathrm{d}x\mathrm{d}y\mathrm{d}z$, $R_{i,j,k}$ is the non-viscous term and $R_{Vi,j,k}$ is the viscous term,

$$R_{i,j,k} = R_{i+1/2,j,k} - R_{i-1/2,j,k} + R_{i,j+1/2,k} - R_{i,j-1/2,k} + R_{i,j,k+1/2} - R_{i,j,k-1/2}, \tag{3}$$

$$R_{Vi,j,k} = R_{Vi+1/2,j,k} - R_{Vi-1/2,j,k} + R_{Vi,j+1/2,k} - R_{Vi,j-1/2,k} + R_{Vi,j,k+1/2} - R_{Vi,j,k-1/2}. \tag{4}$$

The difference scheme is finite volume method. Second order upwind TVD scheme is used to discretize the non-viscous term and the integral method to resolve viscous stress of the momentum equation and energy equation in order to avoid numerical singularity near the solid wall and maintain conservation of the diffusive term.

Let us be back to integral equation (1). The stress tensor is expressed by

$$\boldsymbol{\varepsilon} = \begin{bmatrix} 2\dfrac{\partial u}{\partial x} & \dfrac{\partial v}{\partial x} + \dfrac{\partial u}{\partial y} & \dfrac{\partial w}{\partial x} + \dfrac{\partial u}{\partial z} \\ \dfrac{\partial u}{\partial y} + \dfrac{\partial v}{\partial x} & 2\dfrac{\partial v}{\partial y} & \dfrac{\partial w}{\partial y} + \dfrac{\partial v}{\partial z} \\ \dfrac{\partial w}{\partial x} + \dfrac{\partial w}{\partial y} & \dfrac{\partial w}{\partial y} + \dfrac{\partial v}{\partial z} & 2\dfrac{\partial w}{\partial z} \end{bmatrix}. \tag{5}$$

Assume n is the unit vector normal to the integral surface, then $\mathrm{n} = n_x \mathrm{i} + n_y \mathrm{j} + n_z \mathrm{k}$. We have

$$\boldsymbol{\varepsilon} \cdot \mathrm{n} = (\mathrm{n} \cdot \mathrm{grad}\, u)\,\mathrm{i} + (\mathrm{n} \cdot \mathrm{grad}\, v)\,\mathrm{j} + (\mathrm{n} \cdot \mathrm{grad}\, w)\,\mathrm{k} + n_x \cdot \mathrm{grad}\, u + n_y \cdot \mathrm{grad}\, v + n_z \cdot \mathrm{grad}\, w. \tag{6}$$

For any scalar ϕ, the gradient is defined by

$$\mathrm{grad}\,\phi = \lim_{V \to 0} \frac{\oint \phi \mathrm{d}S}{V}. \tag{7}$$

So we get the gradient expression on a tiny six surface body

$$\mathrm{grad}\,\phi = \frac{1}{V} \sum_{l=1}^{6} \phi_l S_l, \tag{8}$$

where V is the volume of the tiny body, $\mathrm{d}S$ is integral tiny area, S_l is the area vector on every tiny area, and ϕ_l is ϕ value on the Lth area, which can be replaced by Roe average. Then we have

$$\mathrm{grad}\,\phi \approx \frac{1}{V}\left[\sum_{l=1}^{6} \phi_l S_{lx}\,\mathrm{i} + \sum_{l=1}^{6} \phi_l S_{ly}\,\mathrm{j} + \sum_{l=1}^{6} \phi_l S_{lz}\,\mathrm{k}\right]. \tag{9}$$

Here we use u, v, w to replace ϕ,

$$\boldsymbol{\varepsilon} \cdot \mathrm{n} = \mu \frac{\partial \mathrm{q}}{\partial n} + \mu \cdot \mathrm{grad}\, q_n. \tag{10}$$

Considering $p + (2/3)\mu \mathrm{div}(\mathrm{q})$ in Eq. (1), we use the definition of divergence

$$\mathrm{div}(\mathrm{q}) = \lim_{V \to 0} \frac{\oint (\mathrm{n} \cdot \mathrm{q})\,\mathrm{d}S}{V} \tag{11}$$

The viscous stress working on the tiny body in a unit time is

$$(\boldsymbol{\varepsilon} \cdot \mathrm{n}) \cdot \mathrm{q} = \mu\left[\frac{\partial \mathrm{q}}{\partial n} + \mathrm{grad}\, q_n\right] \cdot \mathrm{q}. \tag{12}$$

The quantity of heat flowing into the tiny body is

$$C\frac{\partial}{\partial n}(p/\rho)\,\mathrm{d}s = C\mathrm{n} \cdot \mathrm{grad}(p/\rho). \tag{13}$$

In order to verify the accuracy of the simulation, we compare the simulation result with that of a hypersonic vehicle experiment at the same Mach number and compressive angles. The experimental and simulation condition is that Mach number $M_\infty = 5$ and attack angle $\alpha = 6^\circ$. Fig. 1 and Fig. 2 are the experimental photo and the numerical contour of pressure of a hypersonic vehicle, respectively. The shock system shows well agreeable. Table 1 provides the value of the pressure coefficient at the same position of the forebody. We find that the error is about 1 % between experiment and simulation. So we can ensure that the numerical method we used is suitable.

Table **1** Result comparison of experiment and simulation

Attack angle α	4°	6°	10°
Experiment C_p	0.082 5	0.112 0	0.184 8
Simulation C_p	0.083 4	0.110 5	0.186 7
Error	1.12 %	1.47 %	1.08 %

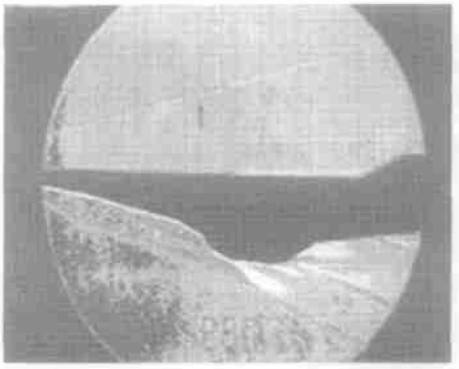

Fig. 1 Experimental picture of the hypersonic vehicle

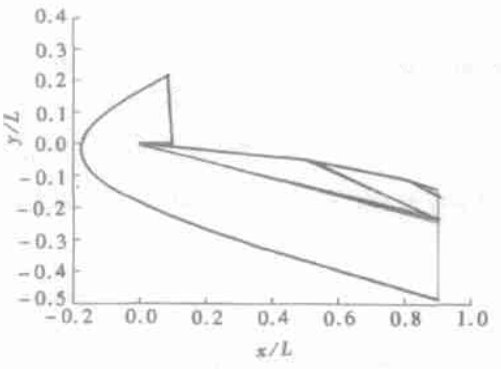

Fig. 2 Pressure contour of simulation

2 Results and Discussions

2.1 The effect of forebody on the inlet performance

For the cruise vehicle at design condition Mach number $M_\infty = 5$, we will discuss the variation of the evaluative flow parameters such as flux coefficient, total pressure recovery coefficient and average Mach number etc at the entry of the inlet, on the base of which we will probe into the mechanism of the effect of forebody on the performance of the inlet. Pressure coefficient C_p denotes the magnitude of pressure of the lower surface of the airframe. Flux coefficient σ is the relative variation of the stream tube area from upstream to the entry of the inlet. According to mass conservation law, there is an equivalent area (A_1) at the entry of the inlet and the free flow (A_∞). So we obtain $\sigma = \rho u/(\rho u)_\infty = A_\infty/A_1$. Total pressure recovery coefficient η is the ratio of total pressure at the entry of the inlet and that of the free flow. It reflects the energy loss flowing along the forebody. There has $\eta = p_{02}/p_{01}$. Uniformity ε of the flow field at the entry of the inlet is also an important parameter for the performance of the inlet and operation of the engine, where $\varepsilon = \sum_{j=1}^{n} \sqrt{(M_j - \bar{M})^2}/(n \times \bar{M})$.

In this paper, we simulated three models including arc model (Model 1), one-order compressive ramp model (Model 2) and two-order compressive ramp model (Model 3) that the compressive angle of the first-order ramp is 4° and that of the second is 5°.

Figure 3 shows the pressure coefficient of the three models. It can be seen that the pressure coefficient is nearly a constant for the one-roder model and increasing slowly for the arc model. Model 3 is different from the former two. Its value augments steply. It is well-known that the pressure coefficient contributes to the lift/drag ratio of the vehicle, so we can find that the two-order compressive model has the advantage to increase pressure coefficient.

The displacement thickness of the three models is shown in Fig. 4 , which denotes the mass loss of the flow. From the figure we can see that this value is not very different from each other at the entry of the inlet.

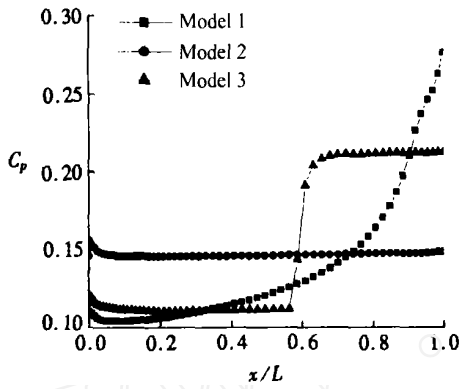

Fig. 3 Pressure coefficient curve

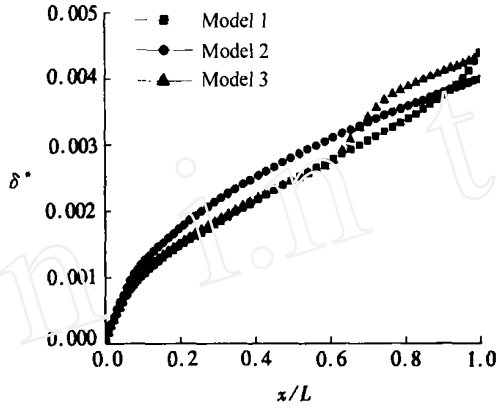

Fig. 4 displacement thickness curve

Table 2 lists the evaluative parameters at the entry of the inlet for the three models. The values of the flux coefficient of Model 1 and Model 3 are higher than that of Model 2. The former two are 2.921 and 3.007 respectively and the latter is only 2.478. The magnitude of the total pressure recovery coefficient has the same order with the flux coefficient. From the view of average Mach number and uniformity of the flow field , Model 3 has dominant advantage. Being compressed by two compressive ramps , the flow field becomes good uniformity and lower Mach number. Additionally , Model 3 also has thinner boundary layer thickness.

Model 2 is not a good model for its low flux coefficient and total pressure recovery coefficient. Model 1 has higher flux coefficient and total pressure recovery coefficient , but its uniformity of flow field and boundary layer thickness are both dissatisfactory. Comparing the three models we can conclude that Model 3 is a suitable model for hypersonic vehicle design.

Table **2** Evaluative parameters at the entry of the inlet

Model	Model 1	Model 2	Model 3
Flux coefficient σ	2.921	2.478	3.007
Total pressure recovery coefficient η	8.301×10^{-1}	7.574×10^{-1}	8.144×10^{-2}
Boundary layer thickness δ	1.354×10^{-2}	1.033×10^{-2}	1.036×10^{-2}
Average Mach number $\bar{M}$	3.251	3.429	3.332
Uniformity of the low field ε	0.279	0.249	0.236

2.2 Effect of the Attack Angle

Using Model 3 as the research object , we made numerical simulation at different attack angles and analyzed the affection on the evaluative parameters. Fig. 5 ~ Fig. 10 depict the variation of the pressure coefficient , flux cefficient , total pressure recovery coefficient , the average Mach number and the lift/drag ratio , which is calculated with the two dimensional model

of the two-compressive model, with the increasing of attack angle. The pressure coefficient at the surface of the airframe increases as the attack angle rises, which shows that attack angle has important affection on the eompressibility of the model. Simultaneously through Fig. 6 and Fig. 7 we can see that the flux coefficient changes from 2.051 to 3.542 when the attack angle rises from 0° to 10°. However the total pressure recovery coefficient, which denotes the mechanical loss, decreases from 0.912 to 0.688 with the increasing of the attack angle. The reason is that the head shock is enhanced when the attack angle is rising, while energy loss of the flow across the shock is augmented. The lessening of the total energy induces the decreasing of the total pressure recovery coefficient. Furthermore we find that the decreasing rate of the total pressure recovery coefficient enlarges while the increasing rate of the flux coefficient decreases when we raise the attack angle, while the lift/drag ratio increases at the same time. There is no evident difference for the uniformity of the flow field and the boundary layer thickness at attack angle of 6° and 10°. At attack angle of 0°, the boundary layer thickness is a little thinner but the uniformity is not as good as that of the other attack angles. Based on the analysis above, we know that attack angle also affect the quality of the flow field. At a range of the attack angle we can get good pre-compressibility, uniformity and thinner boundary layer thickness.

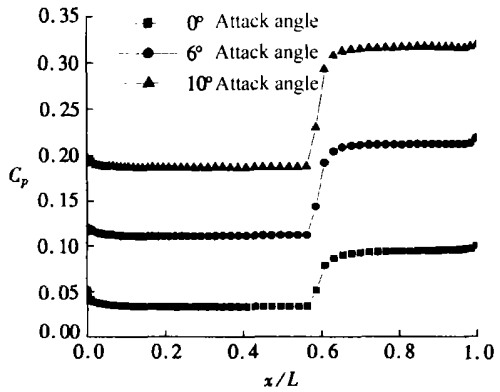

Fig. 5 Pressure coefficient curve

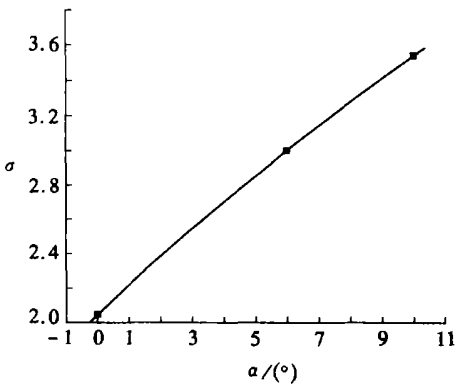

Fig. 6 flux coefficient curve

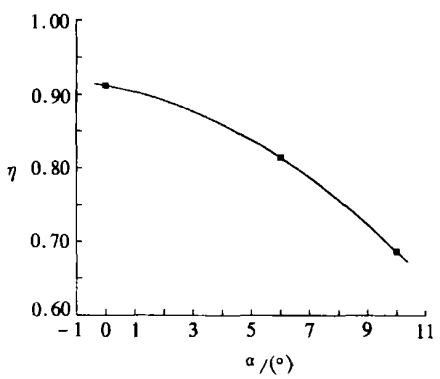

Fig. 7 Total pressure recovery coefficient

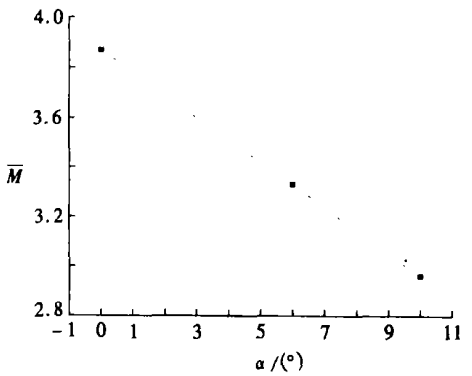

Fig. 8 Average Mach number

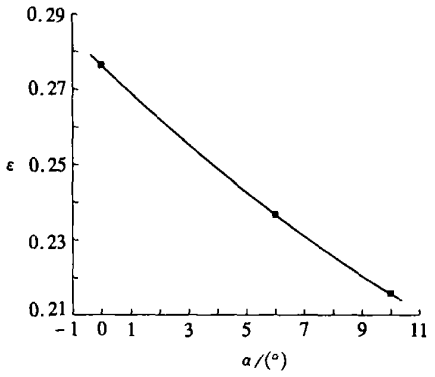

Fig. 9 The uniformity of the flow field

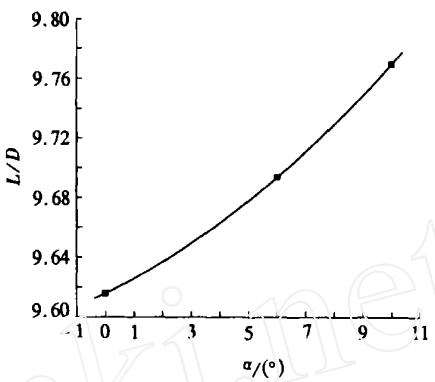

Fig. 10 The lift/drag ratio curve

Table 3 Boundary layer thickness

Attack angle α	0°	6°	10°
Boundary layer thickness	8.015×10^{-3}	1.036×10^{-2}	1.036×10^{-2}

2.3 The effect of combination of compressive angles

In order to study the affection of the forebody on performance of the inlet further, we select four models of the first compressive angle 4° and the second 5°, 5° and 4°, 2° and 7°, and 7° and 2° combinations to analyze. Fig. 11 and Fig. 12 are the pressure coefficient curve and the displacement thickness curve of the four models. Table 4 lists the other evaluative parameters. Different combinations have different values of pressure coefficient, but the boundary layer thickness is nearly the same at the entry of the inlet. Model 5°-4° and Model 4°-5° both have better pre-compressibility, but Model 4°-5° has higher total pressure recovery coefficient than those of Model 5°-4°. When the first compressive angle is raised to 7°, the total pressure recovery coefficient and flux coefficient decreases obviously, which affect the total compressibility greatly. When the second compressive angle is raised, the average Mach number is bigger, which brings difficulty to the engine design. So the Model 4°-5° is the best selection of the forebody design for a designer.

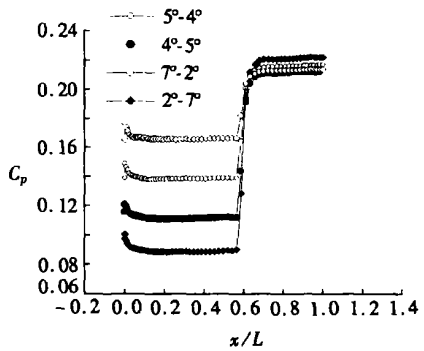

Fig. 11 Pressure coefficient

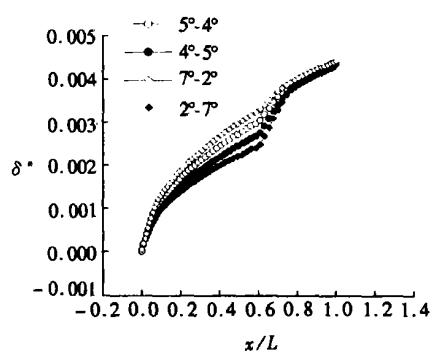

Fig. 12 Displacement thickness

Table **4** Comparison of the evaluative parameters of the four models

Model	Model 5°-4°	Model 4°-5°	Model 7°-2°	Model 2°-7°
Flux coefficient σ	3.004	3.001	2.921	3.027
Total pressure recovery coefficient η	7.720×10^{-1}	8.144×10^{-1}	7.234×10^{-1}	8.386×10^{-1}
Boundary layer thickness δ	9.974×10^{-3}	1.036×10^{-2}	9.658×10^{-3}	1.061×10^{-2}
Average Mach number $\bar{M}$	3.351	3.431	3.311	3.425
Uniformity of the flow field ε	0.231	0.237	0.230	0.236

3 Forebody/Inlet Integrated Design

Based on the above work we accomplished the integrated design of the forebody/inlet. Firstly we should confirm compressive angle and the inlet ramp. Here the first compressive angle is 4° and the second 5° and the inlet ramp angle is 8°. Secondly confirm the position of the inlet cowl, where the shock generated by the forebody and the inlet ramp converge. At the condition of design Mach number $M_\infty = 5$ and attack angle $\alpha = 0°$, we can resolve the first oblique shock through the relation between the Mach number and the shock deflexion angle,

$$\tan\theta = 2\cot\beta\frac{M^2\sin^2\beta - 1}{M^2(\gamma + \cos2\beta) + 2}, \tag{14}$$

where θ is the shock deflexion angle, β is the shock angle and M is the Mach number of the free flow. Then we can get the second and the third oblique shock with Eq. (14) too. The location of the inlet cowl is at the cross of the three oblique shock. The pressure ratio before the shock and after the shock can be educed by the oblique shock relation as follows:

$$\frac{p_2}{p_1} = 1 + \frac{2\gamma}{\gamma + 1}(M_1^2\sin^2\beta - 1), \tag{15}$$

where subscript 2 denotes the value after the shock and 1 before the shock. During the design we should take the rule of equal pressure ratio, i.e. the pressure ratio is approximately the same at each shock.

Lastly we must confirm the area of the throat section of the inlet. Assuming that the area at the entry of the inlet is A_1 and that of the throat is A_2, according to the mass conservation law, the area ratio equation is as follows:

$$\frac{A_2}{A_1} = \frac{M_1}{M_2}\left(\frac{1 + \frac{\gamma - 1}{2}M_2^2}{1 + \frac{\gamma - 1}{2}M_1^2}\right)^{(\gamma+1)/2(\gamma-1)}. \tag{16}$$

In Eq. (16) the Mach number M_1 at the entry of the inlet is obtained from the oblique shock relation, the Mach number M_2 at the throat is given by the performance request of the inlet design.

The last work of this paper is the numerical simulation of the integrated model of the forebody/inlet. The control equation is N-S equation and the numerical method is finite volume method. Fig. 13 shows the shock system of the integrated model by the numerical method. From the numerical result we can get the evaluative parameters. The average Mach number at the entry of the inlet is $\bar{M}_1 = 2.98$. Flux coefficient at the throat of the inlet is $\sigma = 1.58$ and the average

Mach number is $\overline{M}_2 = 2.54$ at the same position. Total pressure recovery coefficient is $\eta = 0.64$ there. It shows that our integrated model has excellent pre-compressibility. The shocks of the forebody converge at the edge of the cowl of the inlet which increases the capture mass greatly and provides a good flow field for the inlet.

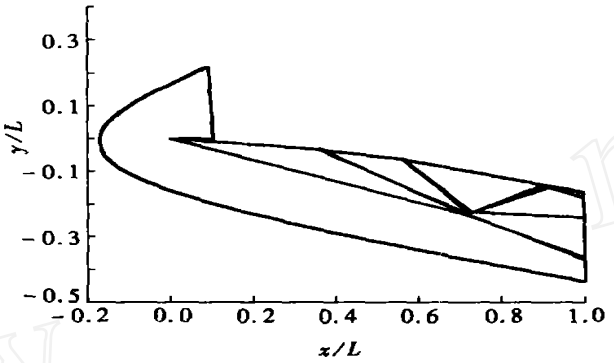

Fig. 13 Shock wave system of the integrated model

4 Conclusions

Based on the above work about the compressibility of the forebody and the integrated design, we have the following conclusions:

(1) The multi-compressive model is a reasonable and useful selection for hypersonic vehicle configuration, with which we can get necessary pre-compressibility and good quality of the flow field.

(2) The attack angle affects the flow field flowing of the forebody greatly. At a range of attack angle we can get high pre-compressive coefficient, uniform flow field and thinner boundary layer thickness.

(3) The combination of the compressive angle is an important factor for the pre-compressibility. Among the models provided by this paper Model 4°-5° is the best configuration for its better flow quality and compressibility for the integrated design of the forebody/inlet.

References:

[1] Kobyashi Hiroaki, Sato Tetsuya, Tanataugu Nobuhiro. Optimization of airbreathing propulsion system for the TSTO spaceplane[R]. AIAA, 2001-1912.

[2] Tsuchiya T, Mori T, Maita M. An integrated optimization for conceptual designs of airbreathing launch TSTO vehicle[R]. AIAA, 2001-1902.

[3] Ryan P, Starkey Mark, Lewis J. Critical design issues for airbreathing hypersonic waverider missiles [J]. Journal of Spacecraft and Rockets, 2001, **38**(4): 510 - 519.

[4] von Eggers Lael, Rudd Darryll, Pines J. Integrated propulsion effects on dynamic stability and control of hypersonic waveriders[R]. AIAA, 2000-3826.

[5] James L Hunt. NASA's dual-fuel airbreathing hypersonic vehicle study[R]. AIAA, 1996-4591.

[6] O'Neil M K L, Lewis M J. Design tradeoffs on scramjet engine integrated hypersonic waverider vehicles[J]. Journal of Aircraft, 1993, **30**(6): 943 - 952.

[7] O'Neil M K L, Lewis M J. Optimized scramjet integration on a waverider[J]. Journal of Aircraft, 1992, **29**(6): 1114 - 1121.

[8] Thomas J. Boagar. Dual-fuel lifting body configuration development[R]. AIAA, 1996-4592.